Journal of Electrostatics 106 (2020) 103452

Contents lists available at ScienceDirect

Journal of Electrostatics

journal homepage: http://www.elsevier.com/locate/elstat

Simulation of electrooptical experiments in liquids

S.M. Korobeynikov [a,b], YuA. Kuznetsova [c,*], V.B. Yassinskiy [c]

[a] Novosibirsk State Technical University, Russia
[b] Lavrentyev Institute of Hydrodynamics, SB RAS, Russia
[c] Karaganda State Technical University, Kazakhstan

ARTICLE INFO

Keywords:
Mathematical simulation
Breakdown
Prebreakdown processes
Kerr effect
Phase shift
Space charge

ABSTRACT

The paper describes the simulation of real electrooptical measurements of prebreakdown processes in nitrobenzene. The developed mathematical model corresponds to the geometric and electrical characteristics of the simulated experiments, which allows solving the inverse problem of recovering the process parameters in the tip zone by solving the direct problem. Visualization of the matrix of the computed intensity values allowed us to obtain a picture of the Kerr fringes. The developed modeling method performs estimation of the electric field distribution in the interelectrode gap on the kerrogram. Calculated kerrograms were compared with experimental ones.

1. Introduction

The process of the pulsed electrical breakdown initiation in liquid dielectrics is due to the appearance of phase inhomogeneities near the electrodes. These heterogeneities can be different nature and can affect the development of a breakdown in different ways. Finding out the reasons leading to breakdown is of great scientific and practical interest. This is due to the search for methods to control the electrical discharge and ways to increase the dielectric strength of liquid insulation. The process of discharge formation is influenced by the type of dielectric and its properties, the parameters of the electric field, the geometry of the discharge gap, etc. Currently, there are several models for the development of liquid breakdown: bubbles, microexplosions, ionization, and electro-thermal. Despite numerous studies of electrical breakdown in liquid dielectrics, a unified theory of the growth of discharge structures has not yet been created. This is because the formation of the discharge structure is influenced by a large number of interconnected macro and micro processes, including those dependent on external factors.

The bubble models of the discharge initiation were considered in Ref. [1–5]. Bubbles in nitrobenzene in prebreakdown electric fields [6,7] were registered close to electrodes in emerged space charge zone; injection of a charge is the main cause of the generation of a space charge [8].

The mechanisms of the origin of this charge are not fully understood, including due to the fact that these processes depend on the experimental conditions. The causes of a space charge are [9]: emission and/or electron trapping by electrodes, equilibrium or non-equilibrium dynamics of an electric double layer, the presence of impurities and contaminants, chemical (electrochemical) reactions between the electrode material and the liquid [10–13].

One of the most convenient experimental methods for remotely obtaining unique information about prebreakdown processes in polar and non-polar liquids is the electrooptical Kerr effect [6,14–18].

Electrooptical experiments concerning the phenomena occurring at the prebreakdown stage of electrical breakdown of liquid were described in Ref. [7,8]. Studies were realized using the Kerr effect. The measuring cell was made out of a quartz glass tube into which specially prepared nitrobenzene was poured. The internal diameter of a tube was 15 mm. The electrode system consisted of a point with a radius of curvature of 0.3 mm and a plane with a diameter of 14 mm, was made by the Rogowski profile. The distance from the tip to the plane was 30 mm. Electrode were made of stainless steel (Fig. 1).

In the experiments [7,8], a ruby laser with a rod 120 mm long and 12 mm in diameter was used. 12 mm is the diameter of the active element of the laser (ruby rod). The radius of the collimated probe beam passing through the measuring cell was limited to apertures up to 3 mm in diameter.

By selecting the configuration of the resonator and the power supply of the pulsed lamps of the pumping system, the laser was switched either to a quasi-continuous mode with pulse duration of almost permanent intensity ~300 μs or giant pulses mode. The Q-switching of the laser was passively using a KS-18 light filter. The duration of individual giant

* Corresponding author.
E-mail address: j.kuznetcova@kstu.kz (YuA. Kuznetsova).

https://doi.org/10.1016/j.elstat.2020.103452
Received 24 July 2019; Received in revised form 26 February 2020; Accepted 21 March 2020
Available online 16 April 2020

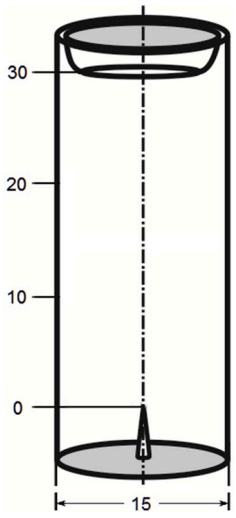

Fig. 1. Sketch of the measuring cell.

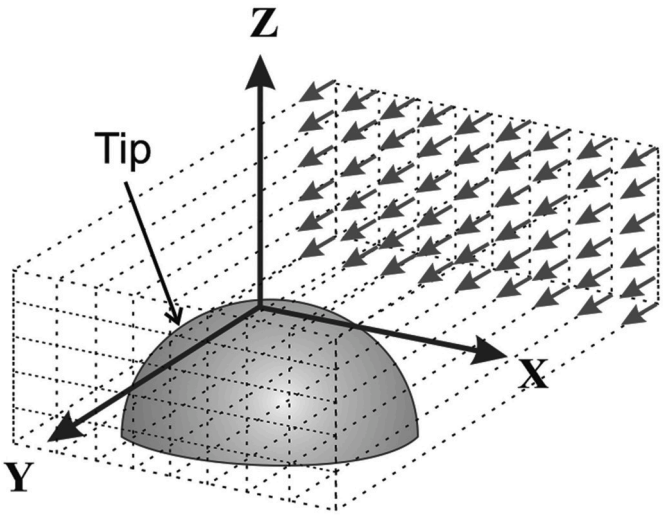

Fig. 2. The geometry of the model.

pulses was at the level of 50–80 ns with an interval from 1 to 40 μs between them.

The registration was made with an SPR-2M camera in a photo recorder mode with a scanning slot oriented along the axis of the electrode system. Frame shooting was implemented by the same camera but without a slot. The SPR-2M characteristics and the specified laser mode allowed spatially separating individual frames with a diameter of 20 mm, which is four times the standard frame-by-frame mode when the frame diameter did not exceed 5 mm.

The results obtained were not fully processed and analyzed due to the lack of an adequate physical and mathematical model of the processes under study and the difficulties of the process itself at that time. Therefore, the construction of a mathematical model, visualization of results using the latest achievements of computer technologies and their comparison with the experiment is relevant.

The goal of our research is to explain the experimental results obtained in Ref. [7,8]. That is why the configuration of a real measuring cell was chosen to construct a mathematical model.

In a number of papers, for example [6,15–19], the Kerr bands have already been calculated in the general case. But the simulation of the conditions of a particular experiment was not conducted.

The problem was solved by the finite element method in a previously constructed 3D model of a real measuring cell. In fact, our method allows us to solve the inverse problem by solving the direct problem. That is, the field of distribution of electrical and dynamic characteristics in the discharge gap is obtained by comparing the real kerrogram with the calculated one.

2. Methodology

In an electric field, nitrobenzene acquires the properties of a uniaxial crystal with an induced optical axis oriented along the direction of the field intensity vector.

If natural light is incident on such a cell perpendicular to the optical axis, it is split into ordinary and extraordinary rays with practically identical intensities.

When the incident light is linearly polarized, birefringence will occur too, but the intensities of the rays will be the same only if the polarization plane of the incident beam is oriented at an angle of 45° to the optical axis. A decrease in the angle (towards 0°) leads to a decrease in the intensity of the extraordinary beam, and an increase in the angle (towards 90°) leads to a decrease in the intensity of the ordinary beam.

Kerrograms are the fringes of an equal phase shift between ordinary and extraordinary rays. Therefore, the redistribution of intensity between these rays can affect the final appearance and contrast of the bands.

In the calculations, the zone adjacent to the tip was sequentially scanned in layers in the XOY plane along the Y-axis with a given step along the X-axis. Then, the scanning plane was shifted along the symmetry axis of the Z cell and the next layer was scanned (Fig. 2).

In the described electrode system, there was a sharp inhomogeneity of the electric field along the path of the probe beam.

If on the way ℓ the orientation of the field does not change and it is constant, then the phase difference between the extraordinary and ordinary rays [8]:

$$\Phi = 2\pi \cdot B \cdot \ell \cdot E^2 \tag{1}$$

If the magnitude of the field changes, but its direction remains unchanged, then on the segment dy the elementary change in the phase difference is:

$$\Phi(y) = 2\pi \cdot B \cdot E^2(y)dy.$$

Then on all the way, ℓ the integral change in Φ is defined as:

$$\Phi = 2\pi \cdot B \cdot \int_0^{\ell} E^2(y)dy \tag{2}$$

Consequently, the problem of determining the distribution of Φ comes down to the calculation of the corresponding integrals $\int_0^{\ell} E^2(y)dy$ over the entire field of interest provided that the orientation of the field (and the optical axis) does not change.

In the case of the nonuniform field when magnitude changes and the angle of rotation of the vector E is small [20], then instead of E you can use its projection $E_{\perp}$ on the Z-axis. Thus, the direction of the induced optical axis is fixed with a predetermined accuracy. Then the expression (2) takes the following form:

$$\Phi = 2\pi \cdot B \cdot \int_0^{\ell} E_{\perp}^2(y)dy \tag{3}$$

Since the transverse size of the computational zone is less than 1 mm with a tube diameter of 15 mm when calculating the integrals $\int_0^{\ell} E_{\perp}^2(y)dy$ we assumed that the geometric paths of all the rays through the measuring cell are the same. The error introduced by the curvature of the walls of the glass tube is vanishingly small and does not affect the final result.

When an electric field is applied to the discharge gap in a

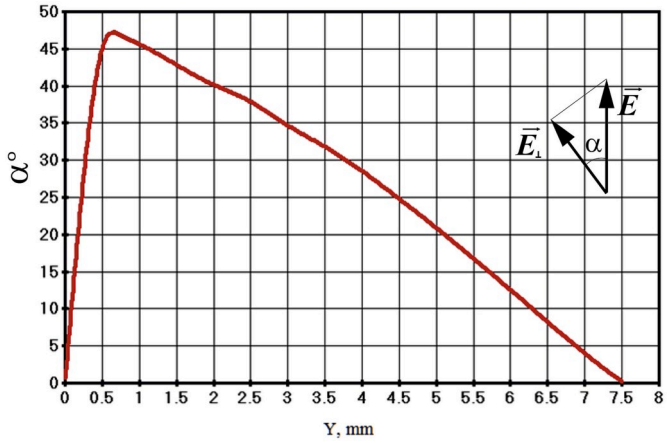

Fig. 3. Changing the angle of rotation of the vector *E* on the path of the beam.

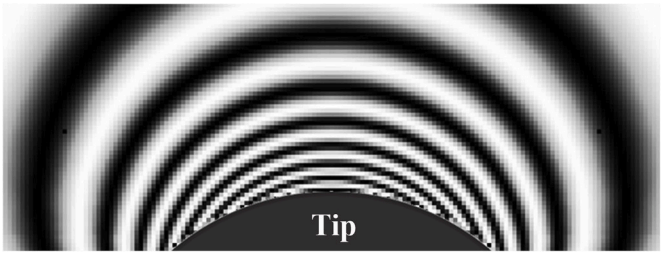

Fig. 4. Computed kerrogram (size 1.0 × 0.4 mm, 1 pixel 5.0 × 5.0 μm).

homogeneous field in nitrobenzene in the measuring cell (Fig. 1), an induced optical axis appears which coincides in direction of the axis of symmetry Z. Due to the arising inhomogeneities in the tip-plane system, the vector orientation E in the path of the probe beam is changing. Therefore, the direction of the induced optical axis changes as well. The impact of this change was assessed. For this, within the framework of the constructed mathematical model [21], we calculated the field profiles (modules of the intensity vector E) and its projections $\boldsymbol{E}_\perp$ on the symmetry axis Z, and using the expression α = arccos ($\boldsymbol{E}_\perp$/E) we determined the rotation angles of the vector E along the entire trajectory a probe beam in the measuring cell (Fig. 3).

The analysis showed that at distances from 0.4 to 1.5 mm from the tip, the *E* vector rotates at an angle close to 45°, which leads to almost extinguishing one of the rays and a sharp decrease in the visibility of the Kerr bands.

Since the induced optical axis is given by the field direction, we have an optical axis that is locally floating in the direction. As a result, as the beam passes across the cell, conditions are permanently changing. Not

Fig. 6. The position of the bubble (d = 20 μm) on the tip (r_0 = 300 μm).

only does the angle between the plane of polarization of the probe beam and the direction of the optical axis change, but also the angle of incidence of the beam on the optical axis.

Estimation of the contribution of one or other part of the path of the beam through the cell, made in Ref. [19], showed that more than 92% of the main contribution to the resulting phase difference between ordinary and extraordinary rays makes just an area extending no further than 0.3 mm from the axis of symmetry to direction of the Y-axis. Therefore, the calculation error lies at the level of 5–8%, which is quite acceptable for such calculations.

Finely, the intensity of the laser beam after passing through the optical inhomogeneity at the exit from the Kerr cell is determined by the law:

$$I(x,z) = I_0 \cdot \sin^2\left(\pi \cdot B \cdot \int E_\perp^2(y)dy\right),$$

and the phase shift is as:

$$\Phi(x,z) = 2\pi \cdot B \cdot \int_{\ell_1}^{\ell_2} E_\perp^2(y)dy.$$

For each direction of the probing laser beam along the Y-axis, the normalized intensity value $I\ (x,z)/I_0$ were computed over all layers. A two-dimensional matrix ||z, x|| was formatted in the whole field of observation. Visualization of the obtained matrix allowed us to obtain a picture of the Kerr bands (Figs. 4 and 5*a*).

3. Microbubbles

One of the mechanisms of electrical breakdown in liquid dielectrics is the so-called bubble mechanism. In microbubbles with a gas [6,22–24], which are located on the electrodes even before the field is applied, ionization processes occur, which lead to their deformations and the nucleation of primary plasma channels. This initiation mechanism is most likely to occur in non-degassed and polar liquids.

The proposed method of modeling allows us to consider the analyzed area including bubbles, with any desired resolution. Therefore, to simulate such a situation, a bubble with a diameter of 20 μm was placed on the surface of the tip (Fig. 6) (see Fig. 7).

Two options were considered: an air bubble without charge and an ionized bubble. The spatial resolution was improved, and the

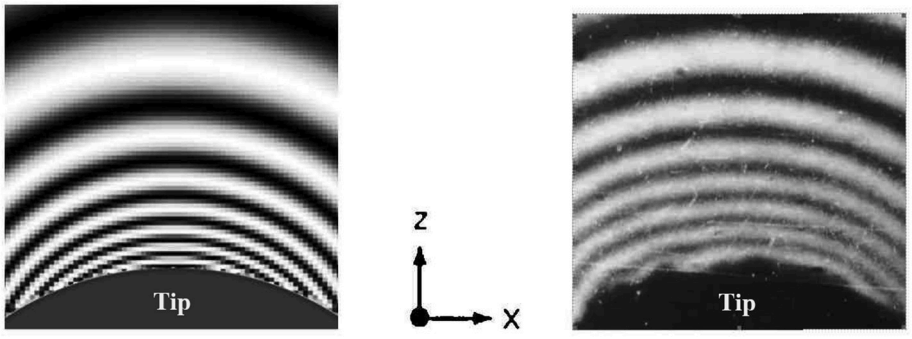

Fig. 5. Examples of kerrogram reduced to the same size and voltage:
(*a*) — calculated, (*b*) — experimental [2].

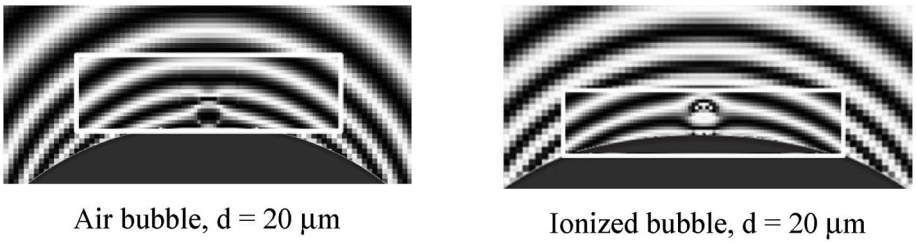

Fig. 7. Kerrograms calculated with are the solution of 5 μm. The selected areas in the near-electrode zone have a resolution of 2.5 μm. Voltage 120 kV. The radius of the tip of the electrode is 300 μm.

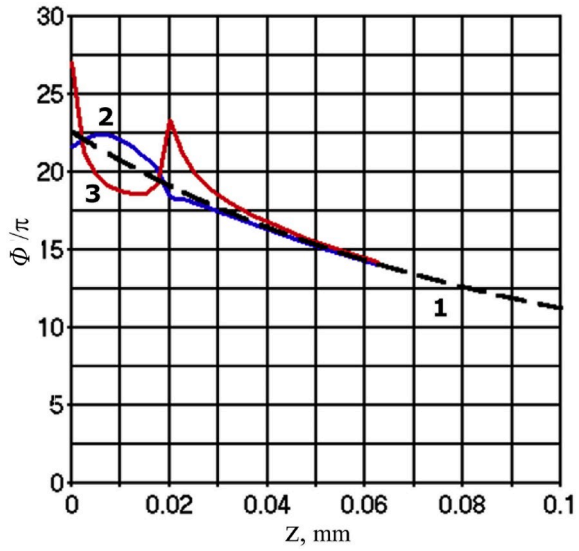

Fig. 8. Phase shift Φ/π depending on z: 1 — the unperturbed interval between electrodes; 2 — with an air bubble; 3 — with ionized bubble.

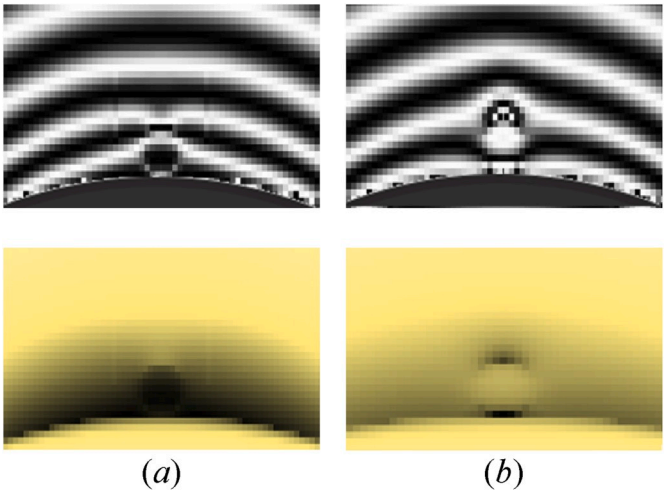

Fig. 9. Calculated kerrograms and phase shift distribution in the area near the tip in case of the dielectric bubble (*a*) and ionized bubble (*b*).

calculations were carried out in 2.5 μm computation step (Fig. 7).

The dependences $\Phi/\pi = f(z)$ constructed from the calculation results (see Fig. 8) permits us to trace in detail the influence of bubbles on the change in the field. The boundary of bubbles is visible (z = 0.02 mm). The electric field near the bubble changes in comparison with the case of its absence. But at a distance of 0.06 mm from the tip of the perturbation, this difference practically disappears and the field becomes the same with the unperturbed state. With the known law of voltage variation at the discharge gap, the calculated step by step record frame allows determine the instant of onset of ionization in the air microbubble by the rupture of the Kerr stripes (Fig. 9).

Analysis of the images obtained (Fig. 9) shows that there is a strong deformation of the Kerr bands closest to the bubble, which makes it possible to detect both the presence of bubbles and their state. This fact is confirmed by photo scanning [7, Fig. 1.13, p. 39] from a series of simulated experiments.

4. Space charge

But even if there are no unknown inclusions, in the system the "tip-plane" near the tip the field is sharply inhomogeneous. Therefore, it is precisely here that a region with a space charge, which significantly distorts the field, can appear. In this region, in liquid dielectrics, the space charge can be formed both coinciding in sign with the electrode, and of the opposite sign. There are many mechanisms of space charge formation; they were investigated, in particular, in Ref. [7,10,11]. In the experiments simulated by us, the mechanism of space charge appearance was investigated in [7, p. 38]. The authors showed by experimental that when the field strength reached of 0.5 MV/cm at the cathode and 1 MV/cm at the anode, the formation of a space charge at the tip occurs due to the emission of charge carriers from the electrodes. In this case, the field of the emitting electrode decreases. At this stage of the study, we assumed that the space charge is homogeneous, is located near the tip, covers it (Fig. 13) and had the sign of the tip.

As a result of the inhomogeneities that appear, the phase difference between the ordinary and extraordinary rays changes, this is reflected in the visual of the picture of the Kerr patterns. In the initial stage of the breakdown development process, the charge value increases with increasing voltage. Changes in the field structure in the tip area are also available.

The calculations showed that in the simulated electrode cell near the tip at 120 kV the field strength reaches a value of $\sim 10^8$ V/m. In real experiments, the surface of the tip is not ideal; therefore, local points with increased field strength should be observed. These fields can reach such a size that the autoionization of liquid molecules occurs. The determining mechanism of this process at the anode may be a tunnel effect [7, p. 338]. At the cathode, an electron emission mechanism is possible. But, in our opinion, the most likely may be the injection of a charge from a double electric layer near the electrode. In all cases, an induced charge appears near the tip, and the field is distorted.

First, the field strength distribution along the Z-axis for the case of space charge was considered.

The computations showed that an increase in the space charge almost proportionally reduces the magnitude of the field near the tip. Besides, when the density of the space charge is higher than 120 C/m^3, the maximum electric field is carried into the gap, to the bound of the space charge region.

The simulation technique used made it possible to consider the behavior of the phase difference Φ under the same conditions.

It attracts attention that both types of dependencies (Figs. 10 and 11)

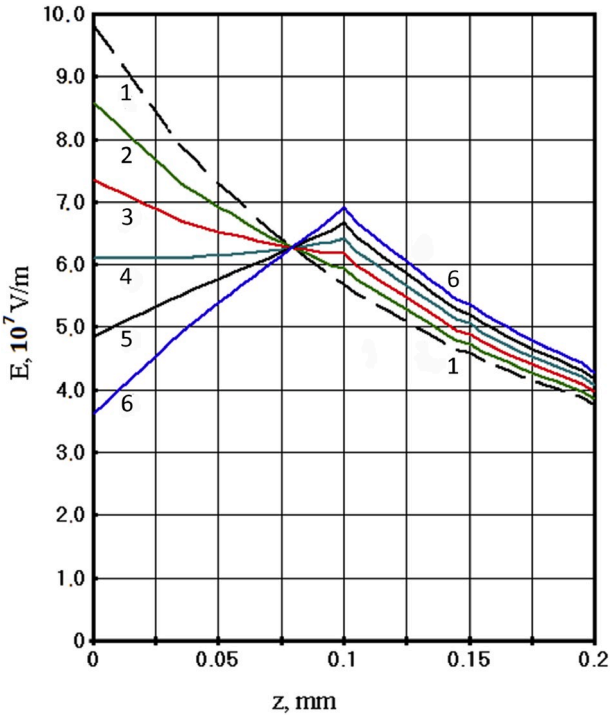

Fig. 10. The dependence of E on the distance z to the tip for a set of homogeneous charges with space density: 1–0 C/m^3, 2–40 C/m^3, 3–80 C/m^3, 4–120 C/m^3, 5–160 C/m^3, 6–200 C/m^3.

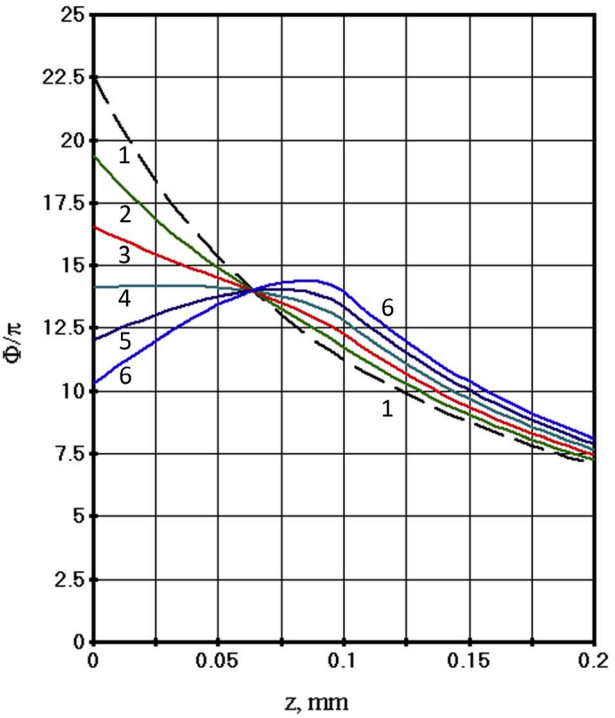

Fig. 11. The dependence of Φ on the distance z to the tip for a set of homogeneous charges with a space charge density: (numbering from top to bottom at z = 0): 1–0 C/m^3, 2–40 C/m^3, 3–80 C/m^3, 4–120 C/m^3, 5–160 C/m^3, 6–200 C/m^3.

are similar to each other. Both the phase difference between the ordinary and extraordinary rays, and the law of change of the electric field intensity have the same features in the behavior. Analyzing both types of dependences of *E* and Φ on z, one can say that if denote the boundary of

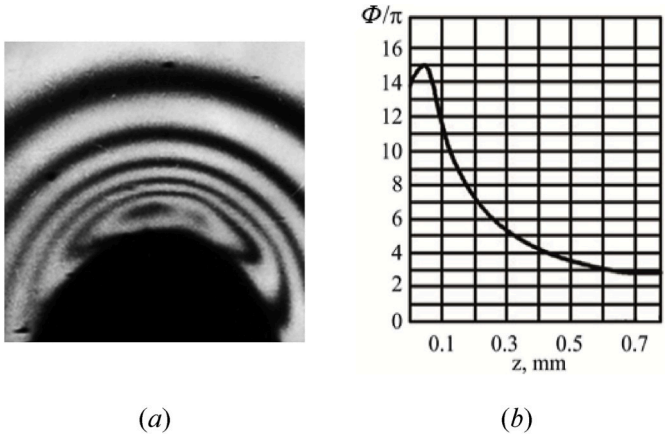

Fig. 12. Experimental kerrogram (*a*); phase shift distribution restored from the kerrogram (*b*).

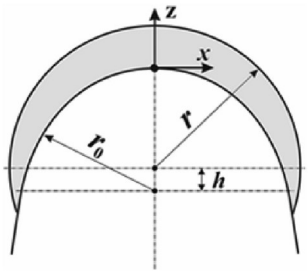

Fig. 13. The layout of the enveloping of the volume charge.

the space charge z_0, then the maximum Φ is reached, depending on the value of the space charge, at a distance from $z_{max} = 0.7\ z_0$ to $z_{max} = 0.8\ z_0$.

A quantitative comparison of the calculated and experimental data could be fulfilled with the developed mathematical model.

Fig. 12*a* demonstrates an experimental kerrogram [6] obtained near a cathode tip with a radius of curvature r = 300 μm at a voltage of U = 135 kV. This picture shows the moment when the field strength in the cathode region reaches the threshold value and the emission of charge carriers begins. This is manifested in the fact that the fringes appear characteristic bends. The thickness and mutual arrangement of the fringes in the emission zone differ significantly from the distribution of the fringes outside it, and it is in this area that the electric discharge will develop. The distribution of the phase shift (Fig. 12*b*) is characteristic of the threshold voltage at which discharge from the point cathode begins.

The picture in Fig. 12*a* was made at a voltage of 135 kV. However, to prevent the measurement cell from destroying in that series of experiments, a protective capacitance was sequentially installed with the electrode gap [7,8]. As a result, when the division factor was 0.89 of the obtained capacitive divider with a generator voltage of 135 kV, the output voltage at the Kerr measuring cell was 120 kV. It is for this voltage that the calculations were made. At the first stage, we restricted ourselves to the consideration of a fixed zone of an emerging space charge. This area (Fig. 13) is directly adjacent to the tip, enveloping it at the rounding.

With a tip radius of $r_0 = 0.3$ mm, the radius of a spherical region with a space charge was taken 0.32 mm. The centers of these spheres are shifted by h = 0.1 mm. That is, on the axis of symmetry the thickness of the layer (0.1 mm) of the charged area is greater than in other places. This is logical from the point of view of the distribution of the field in the area.

Calculations were realized for a set of values of a homogeneous charge at a cell voltage of 120 kV and a fixed area of charge placement

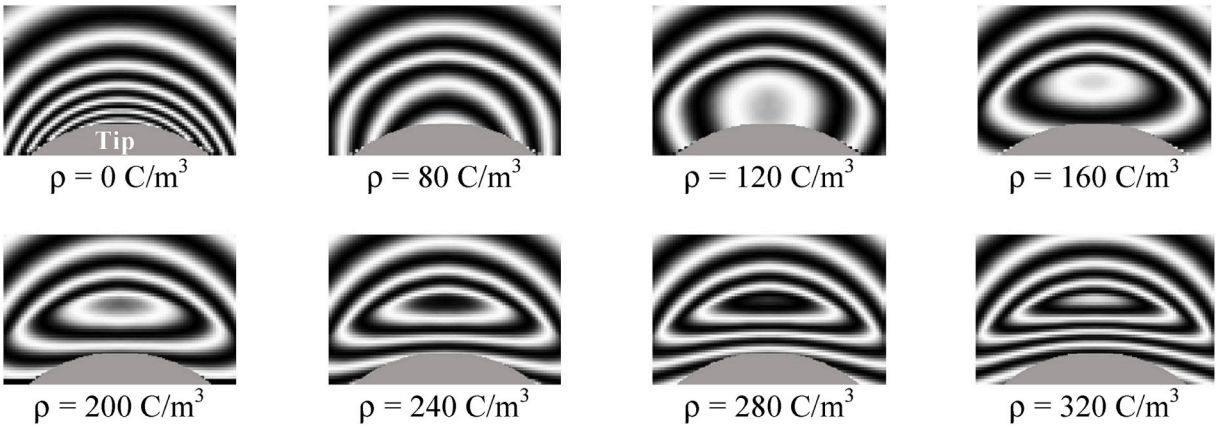

Fig. 14. Simulated kerrograms for a set of homogeneous charges with different space density.

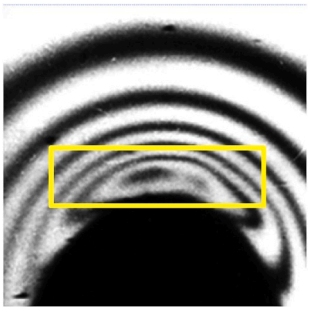

Fig. 15. Experimental kerrograms with the analyzed fragment.

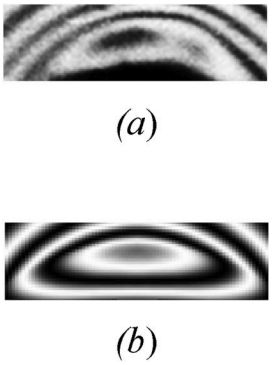

Fig. 16. Comparison of experimental (a) and simulated (b) fragments.

(Fig. 14). The space charge density ρ varied from 0 C/m^3 to 320 C/m^3 in 40 C/m^3 increments.

Despite a certain difference, the calculated kerrograms (Fig. 14) was the closest in appearance to the experimental one (Fig. 15 and 16), corresponding to ρ = 200 C/m^3.

A decrease or increase in the density of the charge from 200 C/m^3 leads to the calculated kerrograms (Fig. 14), which differ radically from the experimental one shown in Fig. 10*a*.

A rough estimate of the value of the space charge from the experimental kerrogram from Fig. 12*a*, when carried out in [7,8], has given a value about 100 C/m^3. Most likely, it is greatly underestimated and the real assessment is ~160–200 C/m^3. A more accurate value and position of the space charge, as well as better agreement between the computed and experimental kerrograms, can be obtained by completing the calculations for smaller sizes of the charged region than is done in the described series.

Nevertheless, the obtained results make it possible to assess the presence, size, shape, and influence of the space charge on the field by the form of the kerrogram and the distribution of the phase shift.

5. Conclusions

The paper shows the possibilities of the simulation method in the analysis of processes occurring at the prebreakdown stage of the breakdown of liquids. The calculation scheme reproduced the conditions of real electrooptical experiments. As a result, it became possible to solve the inverse problem by solving the direct problem by the method of successive approximations under conditions as close as possible to real ones.

The developed modeling method performs us to estimate the influence of the shape of the electrodes on the distribution of the electric field and potential in the discharge gap. In addition, it is possible to assess how the characteristics of the prebreakdown processes change with regard to the space charge and the presence of microbubbles near the tip.

With the known law of change of the electric field on the measuring cell, it is possible to estimate the change in orientation of the induced optical axis and the contribution of one or another part of the path of the probe beam to the total phase difference.

An increase in spatial discretization (up to fractions of a micrometer) will make it possible to examine in more detail the processes in the near-electrode region.

On the basis of the constructed mathematical model of the processes occurring in a real measuring cell, it becomes possible to increase the amount of information obtained from experimental kerrograms. In particular, it is possible to specify the size, location, and space charge density, as well as to predict the state of the system when any parameter changes.

If the law of voltage variation applied to the discharge gap is known, the dynamics of EHD fluxes can be traced, the effect of microbubbles and partial discharges on the breakdown process can be assessed. High-speed photo (high-speed scan mode) obtained in real experiments can be reproduced.

Declaration of competing interest

We, authors of the paper “Simulation of electro-optical experiments in liquids”, have no a conflict of interests.

Acknowledgements

One of the authors (S.M.Korobeynikov) is grateful to RNF (grant 16-19-10229) for support.

References

[1] C.G. Garton, Z. Krasucki, Bubbles in insulating liquids: stability in an electric field, in: Proc. R. Soc. London, A280, 1964, pp. 211–226.

[2] M.N. Shneider, M. Pekker, Pre-breakdown processes in dielectric fluid in inhomogeneous pulsed electric fields, J. Appl. Phys. 117 (2015) 224902.

[3] V.Y. Ushakov, "Pulsed Electric Breakdown in Liquids" [in Russian], Publishing House of Tomsk State University, Tomsk, 1975.

[4] V.F. Klimkin, Bubble generation model for initiating breakdown from anode in n hexane with quasi uniform electric fields", Proc. 13th Intern. Conf. on Dielectric Liquids. - Nara, Japan (1999) 199–202. – pp.

[5] S.M. Korobeynikov, YuN. Sinikh, Bubbles and breakdown of liquid dielectrics, in: Conference Record of the 1998 IEEE International Symposium on Electrical Insulation, vol. 2, June 7-10, 1998, pp. 603–606, https://doi.org/10.1109/ELINSL.1998.694865. Arlington, Virginia, USA.

[6] S.M. Korobeynikov, E.V. Yanshin, K.V. Yanshin, Experimental evidence of bubble model of discharge initiation, in: Proc. Of the 1998 Int. Conf, On Electrical Insulation and Dielectric Phenomena, Atlanta, 1998, pp. 436–438.

[7] V.Y. Ushakov, V.F. Klimkin, S.M. Korobeynikov, Impulse breakdown of liquids, in: Springer (Ed.), Power Systems, 1 ed., Springer-Verlag Berlin Heidelberg, 2007, p. 397.

[8] S.M. Korobeynikov, E.V. Yanshin, K.V. Yanshin, Optical investigation of prebreakdown processes in insulating liquids, in: Proc. 4th Int. Symp. On High Voltage Engineering, 1983. Athenes.

[9] S.M. Korobeynikov, E.V. Yanshin, K.V. Yanshin, Space charge and prebreakdown bubbles formation near point electrodes under pulse voltage, in: Rec. 8th Int. Conf. On Conduction and Breakdown in Dielectric Liquids, 1984. Pavia.

[10] A.I. Zhakin, Near-electrode and transient processes in liquid dielectrics, Phys. Usp. 49 (2006) 275–295.

[11] S.M. Korobeynikov, A.V. Melekhov, G.G. Furin, V.P. Charalambakos, D.P. Agoris, Mechanism of surface charge creation due to image forces" in, J. Phys. Appl. Phys. 35 (11) (2002) 1193–1196, https://doi.org/10.1088/0022-3727/35/11/315.

[12] A. Denat, Conduction and breakdown initiation in dielectric liquids, in: Proc. ICDL, Trondheim, 2011, pp. 1–11. Norway, Jun. 26-30.

[13] T.J. Lewis, Basic electrical processes in dielectric liquids, IEEE Trans. Dielectr. Electr. Insul. 1 (1994) 630.

[14] N.J. Felici, Liquid flow electrification and zeta-potential in hydrocarbons, J. Electrost. 12 (APR) (April 1982) 369–376.

[15] A. Castellanos (Ed.), Electrohydrodynamics, SpringerVerlag, Wien — New York, 1998, ISBN 3-211-83137-1.

[16] M. Zahn, T. Takada, High voltage electric field and space-charge distributions in highly purified water, J. Appl. Phys. 54 (1983) 4762–4775.

[17] A. Üstündag, T.J. Gungand, M. Zahn, Kerr electro-optic theory and measurements of electric fields with magnitude and direction varying along the light path, IEEE Trans. Dielectr. Electr. Insul. 5 (No. 3) (June 1998) 421–442.

[18] A. Üstündağ, M. Zahn, Comparative study of theoretical Kerr electromagnetic fringe patterns in two dimensional and axisymmetric electrode geometries, IEEE Trans. Dielectr. Electr. Insul. 8 (No. 1) (March 2001) 15–26.

[19] Jian Shi, Qing Yang, Wenxia Sima, Lei Liao, Sisi Huang, Marcus Zahn, Space charge dynamics investigation based on Kerr electro-optic measurements and processing of CCD images, IEEE Trans. Dielectr. Electr. Insul. 20 (2) (April 2013) 601–611, https://doi.org/10.1109/TDEI.2013.6508764.

[20] C. Cassidy and N. Harold "A Kerr electro-optical technique for observation and analysis of high-intensity electric fields", J. Res. Nal. Bur. Stand. (U.S.), 73C (Engr. and lnstr.), Nos1 and 2, 5-13 (Jan.-June 1969).

[21] S.M. Korobeynikov, YuA. Kuznetsova, V.B. Yassinskiy, "Simulation and Analysis of Prebreakdown Processes in Liquids", the International Symposium on Electrohydrodynamics, ISEHD 2019, June , pp. 254–256. St. Petersburg, Russia.

[22] S.M. Korobeynikov, E.V. Yanshin, Model of prebreakdown processes in liquid dielectrics under pulse voltage, in: Conf. Record of the 9th Int. Conf. On Conduction and Breakdown in Dielectric Liquids, 1987, pp. 398–402. Salford.

[23] S.M. Korobeynikov, The role of bubbles in the electric breakdown of liquids: prebreakdown processes, High Temp. 36 (3) (1998) 340–345.

[24] V.V. Glazkov, O.A. Sinkevich, P.V. Smirnov, A spherical bubble in liquid dielectric with an electric field, High Temp. 29 (6) (1991) 884–892.